

Catalytic effect of nano-particle 3d-transition metals on hydrogen storage properties in magnesium hydride MgH₂ prepared by mechanical milling

Nobuko Hanada†, Takayuki Ichikawa‡, Hironobu Fujii ‡*

Graduate School of Advanced Sciences of Matter, Hiroshima University,

1-3-1 Kagamiyama, Higashi-Hiroshima 739-8530, Japan

Natural Science center for Basic Research and Development, Hiroshima University,

1-3-1 Kagamiyama, Higashi-Hiroshima 739-8526, Japan.

hanadan@hiroshima-u.ac.jp

RECEIVED DATE

*corresponding author: E-Mail: hanadan@hiroshima-u.ac.jp, †Graduate School of Advanced Sciences of Matter, ‡Natural Science center for Basic Research and Development

ABSTRACT We examined the catalytic effect of nano-particle 3d-transition metals on hydrogen desorption (HD) properties of MgH₂ prepared by mechanical ball milling method. All the MgH₂ composites prepared by adding a small amount of nano-particle Fe^{nano}, Co^{nano}, Ni^{nano} and Cu^{nano} metals and by ball milling for 2h showed much better HD properties than the pure ball-milled MgH₂ itself. Especially, the 2 mol% Ni^{nano}-doped MgH₂ composite prepared by soft milling for a short milling time of 15 min under a slow milling revolution speed of 200 rpm shows the most superior hydrogen storage

properties: A large amount of hydrogen (~6.5 wt.%) is desorbed in the temperature range from 150 to 250 °C at a heating rate of 5 °C /min under He gas flow with no partial pressure of hydrogen. The EDX micrographs corresponding to Mg and Ni elemental profiles indicated that nano-particle Ni metals as catalyst homogeneously dispersed on the surface of MgH₂. In addition, it was confirmed that the product revealed good reversible hydriding/dehydriding cycles even at 150 °C. The hydrogen desorption kinetics of catalyzed and non-catalyzed MgH₂ could be understood by a modified first order reaction model, in which the surface condition was taken into account.

Hydrogen storage materials, Magnesium hydride, Mechanical milling, catalytic effect, nano-particle metal

1. Introduction, 2. Experimental procedures, 3 Results and Discussion, 3.1 Catalytic effect of nano-particle 3d-transition metals, 3.2 Optimization of milling condition for Ni catalyst, 3.3 Cyclic properties of hydrogenation/dehydrogenation for the 2mol% Ni^{nano} –catalyzed MgH₂ composite, 3.4 Kinetics for hydrogen desorption (HD) reaction in pure MgH₂ and Ni-catalyzed MgH₂ composite, 3.5 Estimation of activation energy in pure MgH₂ and Ni-catalyzed MgH₂ composite, 4. Conclusion

1. Introduction

Magnesium hydride MgH₂ is one of the attractive hydrogen storage materials because it is directly formed from the reaction of Mg metal with gaseous hydrogen and reaches a high hydrogen capacity (~7.6 wt.%). However, the reaction is too slow for practical use and needs higher temperature than 300 °C for progressing hydrogen absorption and desorption reactions [1-3].

Recently, the hydrogen storage (H-storage) properties of the composites composed of Mg or MgH₂ and a small amount of transition metals Ti, V, Mn, Fe, Co, Ni, Cu and Pd or transition metal oxides has been studied to improve the hydriding/dehydriding kinetics without reducing its high hydrogen capacity [4-18].

Liang et al. have reported some good H-storage properties of MgH₂ with 5 mol% transition micro-particle metals (Ti, V, Mn, Fe and Ni) milled for 20 h [4-8], in which the composite with V desorbed ~5 wt.% hydrogen within 200 s at 300 °C under a hydrogen pressure of 0.015MPa. Furthermore, Zaluska et al. have studied H-storage properties of Mg composites prepared by ball milling with 1 wt.% transition micro-particle metals (corresponding to 0.3 mol% Pd and 0.5 mol% Fe doping), and ~6 wt.% of hydrogen was desorbed at 330 °C within 30min (1800 sec) under a hydrogen pressure of 0.1 MPa [9]. They claimed that the doped metals uniformly distributed on the magnesium surface in the form of nano-particles. This indicates that when very small size particles (diameter of several tens nanometers) of the metal catalyst are uniformly distributed on the Mg surface, even a small amount of catalyst is sufficient for improving the reaction kinetics. Recently, Kanoya et al. have investigated H-storage properties of some ball milled Mg with a small amount of nanometer sized metals (Ni and Fe) as catalyst [10]. Their results indicated that a Mg-0.33Ni-0.17Fe (at.%) composite prepared by ball milling for only 15 min could absorb and desorb 7.49 wt.% of hydrogen at 350 °C.

On the other hand, Oelerich et al. have reported some catalytic effects of the transition micro-particle metal oxides for MgH₂ [11-14]. The MgH₂ composites prepared by ball milling for 100 h with 0.2 mol% Nb₂O₅ revealed the best H-storage properties among all the metal oxide catalysts: ~7 wt.% of hydrogen was desorbed within 150 s at 300 °C under vacuum [14].

In our group, it has been clarified that Pd-coated nano-structured Mg films prepared by a RF sputtering method absorbed ~5 wt.% of hydrogen at 373 K under hydrogen atmosphere of 0.1 MPa and completely desorbed below 373 K in vacuum [15-16]. This indicates that MgH₂ is suitable for practical uses as well by modification of bulk MgH₂ into suitable nano-structure and catalyzing with suitable metals on it. In addition, we examined the correlation between H-storage properties and structural characteristics on the mechanically milled MgH₂ itself as a function of milling time, before studying the catalytic effect on H-storage properties of MgH₂ [19]. The results indicated that at the early stage within 2 h milling, the amount of desorbed hydrogen decreased ~16 % from 7.3 to 6.1 wt.% and the onset temperature of dehydrogenation decreased by 70 °C from 400 °C to 330 °C, while both the powder size

and the crystallite size in powder decreased with increasing the milling time down to 1 μm and ~ 10 nm, respectively. On the other hand, the lattice strain of 0.3 % was quickly introduced, but it was completely released after 2 h milling. Finally, after 80h milling the hydrogen capacity and desorption temperature reached to saturation of 6.5wt. % and 330 $^{\circ}\text{C}$, while the crystalline size and the lattice strain reached to saturation for ~ 7 nm and again 0.2 %, respectively.

At the next step of systematic studies of improving H-storage properties in Mg systems, in this paper, we examined the catalytic effect of nanometer-sized 3d-transition metals (Fe^{nano} , Co^{nano} , Ni^{nano} , and Cu^{nano}) on H-storage properties in MgH_2 prepared by mechanically milling method without exposing in air the products in all the preparing and measuring processes. The reason why we used nano-particle size metals as catalyst for MgH_2 is that they can be uniformly dispersed on the surface of MgH_2 by short ball milling and can avoid severe internal strains. As a result of such careful treatments, the obtained results indicated the most superior kinetic properties for hydrogen storage in the MgH_2 composites doped by 3d transition metals so far reported as far as we know.

2. Experimental procedures

Magnesium hydride powder MgH_2 (the purity is 90 wt.%, with several micron meter sizes, 9 wt% is no reacted Mg and the rest of 1 wt% are impurities) was purchased from Sigma-Aldrich. The catalyst nanometer-particle metals Fe^{nano} , Co^{nano} , Ni^{nano} and Cu^{nano} with diameter of several ten nanometers and micro-particle Ni^{micro} with diameter of 3 micrometer were purchased from Shinku-Yakin Company and Rare metallic, respectively. The size of nanometer particles were determined by a TEM sampling method. In those nanometer-particle metals, any existence of the Ni, Fe and Cu oxide phases were not detected by XRD examination. Only Co nano-particles indicated the Co_3O_4 phase in addition to the pure Co metal phase. Prior to milling, the mixture of 300 mg with MgH_2 and 1~2 mol% Fe^{nano} , Co^{nano} , Ni^{nano} , and Cu^{nano} was put into a Cr steel pot (30 cm^3 in volume) together with 20 steel balls (7 mm in diameter). Then, after the pot was degassed below 1×10^{-4} Pa for 12 h, high-purity hydrogen gas (7 N) of 1.0 MPa was introduced into it. After then, the mixture was mechanically milled for 15 min~2 h at

200~400 rpm using a planetary ball milling apparatus (Fritsch P7). The samples before and after milling were always handled in a glove-box filled with purified Ar gas so as to minimize the oxidation on the samples. It is to be noted that this treatment in clean limit is also quite important to avoid surface oxidation.

The morphology of the composite particle was examined by Scanning Electron Microscopy (SEM) observation (Hitachi S-2380N), and metal distribution on the milled particles was detected by the EDX equipment (EMAX-7000). The structural properties were examined by X-ray diffraction measurement (Rigaku RINT2000) using a Cu $K\alpha$ radiation. The hydrogen desorption (HD) properties of the products were examined by a thermal desorption mass spectroscopy (TDMS) (Anelva M-QA200TS) in the heating process up to 450 °C with a heating rate of 5 °C/min under high-purity He gas (purity > 99.9999 %) flow with no partial pressure of hydrogen, in which a thermogravimetry (TG) (Rigaku TG8120) is also equipped. This equipment was specially designed and installed in a glove-box filled with purified Ar gas, so that the measurements of TDMS and TG could be achieved simultaneously without exposing the samples to air.

3. Results and Discussion

3.1 Catalytic effect of nano-particle 3d-transition metals

Figure 1 shows profiles of thermal desorption mass spectra (TDMS) of hydrogen (H_2) for pure non-catalyzed MgH_2 and catalyzed MgH_2 composites with 1 mol% Fe^{nano} , Co^{nano} , Ni^{nano} and Cu^{nano} nano-particle metals prepared by ball milling for 2 h under a hydrogen gas pressure of 1 MPa. It can be seen that all the composites with nano-particle metals as catalyst exhibit better hydrogen desorption properties than the pure MgH_2 by only 2 h milling: Their peak temperatures of hydrogen desorption are lower than that of pure MgH_2 and the amounts of desorbed hydrogen deduced from TG measurement are ~7 wt.% until 450 °C and almost the same as that of pure MgH_2 because only a small amount of nano-particle metals (1 mol%) are added to MgH_2 . Thus, we notice that a small amount of nano-particle metals reveal a significant catalytic effect on the HD properties in MgH_2 without reducing its high

hydrogen capacity. The Ni^{nano}-catalyzed MgH₂ composite shows the best hydrogen desorption properties among all the catalyzed MgH₂ composites and the peak temperature (260 °C) is about 100 °C lower than that of the pure milled MgH₂. In addition, it seems likely that these HD properties depend on the states of 3d-electrons because the peak temperature of hydrogen desorption decreases with increasing a number of occupied 3d-electrons on those transition metals except for Cu, which is known as one of non-catalytic materials from the fact that the 3d-electron shell of Cu metal is fully occupied [20]. In the bottom of Fig. 1, the TDMS profile of the MgH₂ composite milled with 1 mol% micro-particle Ni^{micro} for 2 h is shown, for comparison with that of the 1 mol% Ni^{nano}-doped MgH₂ composite. It is noticed that the latter is much better than the former in the HD properties. This indicates that the smaller particle as a catalytic metal leads to better H-storage kinetic properties by short milling.

Figure 2 shows X-ray diffraction profiles for the MgH₂ composites with 1 mol% Fe^{nano}, Co^{nano}, Ni^{nano} and Cu^{nano}. The main profiles for the above catalyzed samples exhibit the same peaks corresponding to β-MgH₂ and γ-MgH₂ as in the pure milled MgH₂. Except for the Co^{nano}-doped composite, small peaks corresponding to Ni, Fe and Cu metals additionally exist in their patterns. Since the Cu radiation is used in this work, the XRD method is not useful for the Co element in composites because the absorption cross section of Co element is the largest among 4 period elements for the Cu Kα radiation.

3.2 Optimization of milling condition for Ni catalyst

As described above, the Ni^{nano}-catalyzed MgH₂ composite showed the best HD properties among the 3d-transition metal catalyzed composites. For optimizing the milling conditions, we next examined how the HD properties in the Ni^{nano}-catalyzed system are kinetically improved by changing the milling time, the milling revolution speed and the amount of Ni^{nano} catalyst.

First of all, the 1 mol% Ni^{nano}-catalyzed MgH₂ composite was prepared by changing the milling time from 15 min to 2 h at 400 rpm and examined the TDMS profiles. As shown in Fig. 3, the milling for 1 h leads the onset temperature to about 150 °C, while the milling for 15 min leads the peak temperature to about 210 °C as well. Thus, the result indicates that the short time milling brings the better HD

properties by using nano-particle Ni^{nano} as catalyst. However, the TDMS profile shows a shoulder structure and widely distributes in the temperature range from 150 to 300 °C.

At the second step, the milling revolution speed from 400 rpm to 200 rpm was changed under the condition of the short milling time for 15 min. In Figs. 4 (a) and (b), the TDMS profiles are shown for the 1 mol.% Ni^{nano} -catalyzed MgH_2 composite milled at 400 rpm and 200 rpm, respectively. It can be seen that the profile of the composite milled at 200 rpm reveals a single hydrogen desorption peak, but the desorption temperature range still widely distributes from 150 °C to 300 °C.

Finally, the amount of Ni^{nano} catalyst was increased from 1 mol.% to 2 mol.% under the same conditions concerning with short milling time for 15 min and the slow milling revolution speed at 200 rpm. As is shown in Fig. 4 (c), the MgH_2 composite with 2 mol% Ni^{nano} shows the most superior HD profile in the TDMS curves among all the composites examined in this work. Thus, it has been found that the 2 mol% Ni^{nano} -catalyzed MgH_2 prepared by the optimum condition desorbs a large amount of hydrogen (~6.5 wt.%) in the temperature from 150 to 250 °C at the heating rate of 5 °C /min. From these results, it is concluded that the short milling time and slow milling revolution speed brings better HD properties for the 2 mol% Ni^{nano} -catalyzed MgH_2 composite.

To clarify the reason why the HD kinetic properties for MgH_2 are so improved by a small amount of Ni^{nano} catalyst, the EDX micrographs corresponding to the Mg and Ni elemental profiles were examined for the optimum MgH_2 composite, i.e. 2 mol% Ni^{nano} -catalyzed MgH_2 milled for 15 min at 200 rpm, which is shown in Fig. 5. It can be seen that the micrograph pattern of Mg is almost the same as that of Ni. This indicates that the Ni^{nano} -particles uniformly disperses on the surface of the several micron-sized MgH_2 particles by ball milling even for the short time and under the slow milling revolution speed.

3.3 Cyclic properties of hydrogenation/dehydrogenation reactions for the 2 mol% Ni^{nano} -catalyzed MgH_2 composite

Next, the cyclic properties of hydriding/dehydriding reactions were examined for the 2 mol% Ni^{nano} -catalyzed MgH_2 composite prepared by milling for 15 min at 200 rpm. The durability was tested by the

following cyclic processes: the dehydrogenation was performed by keeping the following two different temperatures; (1) 150°C (corresponding to the onset temperature for dehydrogenation) and (2) 200 °C (corresponding to the peak temperature for dehydrogenation) for 12 h under high vacuum, respectively, while the hydrogenation was performed under pure hydrogen gas up to 3 MPa at (1) 150 and (2) 200 °C for 12 h, respectively, as well. After completing those (1) and (2) hydrogen absorbing/desorbing cycles, the HD properties were examined by the TG-TDMS measurement. The results obtained are shown in Fig. 6. The dehydrogenation property after 2nd cycle at 150 °C is better than that after 2nd cycle at 200 °C in a viewpoint of the temperature range of hydrogen desorption and the amount of desorbed hydrogen, but it is slightly worse than that after 1st cycle. As is seen in Figs. 7(a) and (b), the X-ray diffraction profiles indicate that both products after just milling and after dehydrogenating at 150°C have a small peak corresponding to pure Ni-metal phase in addition to the main peaks for MgH₂ and Mg, respectively. On the other hand, as shown in Fig.7(c) for the product after dehydrogenation at 200°C, there are the additional peaks corresponding to the Mg₂Ni phase. Since the catalytic effect of Mg₂Ni for improving the H-storage properties is weaker than Ni-metal, the existence of Mg₂Ni in the Ni^{nano}-catalyzed MgH₂ composite would make the dehydrogenation properties worse.

This may be also the reason why the short milling time and slow milling revolution speed brings the better HD properties for Ni^{nano}-catalyzed MgH₂ in the section 3.2. When the milling time and revolution speed are, respectively, too long and too high, the Mg₂Ni phase could be easily formed at the phase boundaries between Ni and main Mg phases because the affinity of Mg and Ni is very strong with each other. Thus, the formation of Mg₂Ni leads to worse HD properties with increasing the milling time and milling revolution speed for MgH₂ as well.

3.4 Kinetics for hydrogen desorption (HD) reaction in pure MgH₂ and Ni^{nano}-catalyzed MgH₂ composite

In this work, the kinetics of the HD reaction was examined for the 2 mol.% Ni^{nano}-catalyzed MgH₂ and pure non-catalyzed MgH₂ produced by ball milling for 15 min at 200 rpm. Figure 8 shows amount

of desorbed hydrogen as a function of time at ~163 °C and ~308 °C for the catalyzed and non-catalyzed MgH₂, respectively, which were deduced by the TG measurements. It can be seen that the HD curve of Ni^{nano}-catalyzed MgH₂ is of exponential type, while that of non-catalyzed MgH₂ is of sigmoid shape as same as in non-milled MgH₂ itself [25]. In this work, it takes more than 200 min at 308 °C to reach complete hydrogen desorption from non-catalyzed MgH₂ after milling for 15 min. Results in literature indicate that the desorption times of milled MgH₂ are typically between 30-100 min at 300 °C [11,24]. However, it should be noted that all of those data were examined after milling for longer time than 15 min. Therefore, it seems that longer milling leads to better kinetics for non-catalyzed MgH₂ by creating activated surface. On the other hand, after catalyzing by 2 mol% Ni^{nano} on MgH₂, it is noteworthy that 90 % of hydrogen is desorbed within 100 min at 163 °C under He gas flow with no partial pressure of hydrogen, indicating drastic improvement of the kinetics. It should be described in this connection that 90 % of hydrogen is absorbed within 15 min at the same temperature under a hydrogen gas pressure of 3 MPa vice versa.

On the basis of the above results, modified residual hydrogen functions, $F_1(t) = \ln y_1(t)$ and $F_2(t) = -(|\ln y_2(t)|)^{1/2}$ are plotted as a function of time in Fig. 9, where $y_1(t)$ and $y_2(t)$ indicate residual hydrogen concentrations ($0 \leq y \leq 1$) normalized by the hydrogen content at $t = 0$ for the catalyzed and non-catalyzed MgH₂, respectively. It can be seen that both the functions linearly decrease with increasing time, after the sample temperatures have reached the programmed ones of about 163°C and 308°C, respectively. For the Ni^{nano}-catalyzed MgH₂, the good linearity in Fig. 9(a) indicates that the desorbing reaction is a first order one. Huot et al. [5] have so far claimed that the hydrogen desorption reaction for 5 mol% TM^{micro}-doped MgH₂ where TM = Ti, V, Mn, Fe and Ni at 250 °C under 0.015 MPa followed the interface controlling law of $[1 - y^{1/2}] = kt$. Appearance of the first order reaction in this work might be ascribed to the catalytic effect of the nano-particle Ni metal on the sample surface. Generally, it is well-known that the first order reaction obeys the following differential equation,

$$\frac{dy}{dt} = -k y \quad (1),$$

where k is the reaction rate constant, that is, the HD reaction rate is proportional to the residual hydrogen content. On the other hand, for the non-catalyzed MgH_2 , $F_2(t) = -(\ln y_2(t))^{1/2}$ linearly changes as a function of time as shown in Fig. 9(b). This function has been generally expressed as the Johnson-Mehl-Avrami (JMA) equation for a nucleation and growth process [21-23] and the exponent $1/2$ might remind us zero nucleation rate and two dimensional growth of nuclei or a constant nucleation rate and one dimensional growth of nuclei as a rate determining step. In some papers, it has been concluded that the rate determining step of the HD reaction for pure MgH_2 was the nucleation and growth of Mg phase on the basis of similar experimental results to ours [24-25]. In other words, these considerations by means of the JMA equation are based on the dynamics of inner MgH_2 particle like nucleation and growth. However, we have only modified the surface condition of the MgH_2 powder by Ni catalyst and HD reaction was significantly improved and transformed into a first order one. Since Mg has no strong catalytic effect for dissociating H_2 molecule into H atoms on the surface vice versa [26], the recombination process on the MgH_2 surface should be taken into account as a rate determining step of the HD reaction for pure MgH_2 .

Hence, to systematically understand the HD reaction kinetics for non-catalyzed MgH_2 as well as catalyzed MgH_2 , a new HD reaction model is necessary and proposed in this paper. Then, we assume that the HD reaction from MgH_2 to $\text{Mg}+\text{H}_2$ follows a modified first order reaction model, in which a surface condition is taken into account. As the surface condition, we introduce an activated surface area $1 - \theta(t)$ and a non-activated surface area $\theta(t)$ on the non-catalyzed MgH_2 powder, which are normalized by a total surface area. On the activated surface area, we assume that hydrogen atoms are easily recombined into hydrogen molecules and are released into He flow gas. Furthermore, we assume that the non-activated surface area $\theta(t)$ is an exponential type decreasing function for reaction time as follows,

$$\theta(t) = \exp(-\nu t) \quad (2),$$

where ν is a reaction rate constant. Thus, the activated surface area $1-\theta(t)$ increases with time evolution and finally reaches to 1. This assumption suggests that the recombination rate of H_2 on the surface gradually increases with the increasing time by a surface modification during the HD reaction. Microscopic behavior of the surface modification during HD reaction is considered that the MgO layers on the MgH_2 surface are reduced by desorption hydrogen to Mg or the surface structure of non-activated surface is reconstructed to activated surface.

Therefore, the HD rate of non-catalyzed MgH_2 should be proportional to both the normalized residual hydrogen content $y(t)$ and the activated surface factor $1-\theta(t)$, as follows,

$$\frac{dy}{dt} = -ky(1-\theta(t)) \quad (3).$$

By integrating Eq. (3), we can obtain the following expression

$$\ln y = -k \int_0^t [1 - \exp[-\nu t]] dt \quad (4).$$

Actually, in the case of pure milled MgH_2 , we can well fit the desorption reaction by Eq.(4). Here, if $\nu t \ll 1$, then $1-\theta(t)$ is expanded as $1 - \exp(-\nu t) = \nu t - (\nu t)^2/2 + (\nu t)^3/6 \dots \cong \nu t$. Then, Eq.(4) is rewritten as follows,

$$\ln y \cong -k \int_0^t \nu t dt = -\frac{1}{2} k \nu t^2 \quad (5).$$

By transforming Eq.(5), we obtain the following equation, that is the same function as $F_2(t)$

$$F_2(t) = -(\ln y)^{1/2} = at, \text{ where } a = -\sqrt{\frac{1}{2} k \nu} \quad (6).$$

Thus, we can understand the HD reaction of MgH_2 by the modified first order model, in which the surface activation condition is taken into account as well. From the experimental data, we deduced the value of $\nu t_{\max} \cong 0.008$, $t_{\max} = 260$ min, which really satisfies the condition of $\nu t \ll 1$ in the above assumption.

In the case of the Ni^{nano} -catalyzed MgH_2 , we can also understand the HD reaction using the modified first order model. Then, it is considered that the non-activated surface area is $\theta(t) = 0$ at any time,

because 3d-transition metal Ni^{nano} has the strong catalytic effect for recombining H atoms to H₂ molecules. Therefore, the activated surface area is $1 - \theta(t) = 1$ at any time in Eq. (2) and the desorption reaction rate should be described by Eq.(1), being a first order reaction.

3.5 Estimation of activation energy in pure MgH₂ and Ni^{nano}-catalyzed MgH₂ composite

If the HD reaction as a function of time is described by Eqs. (1) and (3), we can estimate the activation energy, E , by the Kissinger method [27] according to the following consideration. In the constant heating process like $T = T_0 + \beta t$, where T_0 is the initial temperature of the reaction and β the heating rate, Eq. (3) (where $1 - \theta(t) \approx \nu t$) for the modified first order reaction is generalized to

$$\frac{dy}{dT} = -\frac{1}{\beta} k y \nu \frac{T}{\beta} \quad (7).$$

Here, k and ν can be respectively expressed by the Arrhenius equation as follows,

$$k(T) = k_0 \exp [-(E_{A1}/RT)] \quad (8), \quad \text{and}$$

$$\nu(T) = \nu_0 \exp [-(E_{A2}/RT)] \quad (9),$$

where k_0 and ν_0 are the frequency factors, R the gas constant, E_{A1} and E_{A2} the activation energies for the HD process with an activated surface and the surface activating process, respectively. By substituting Eqs.(8) and (9) into Eq.(7), we obtain the following equation,

$$\frac{dy}{dT} = -k_0 \nu_0 \exp \left[-\frac{E_{A1} + E_{A2}}{RT} \right] y \frac{T}{\beta^2} \quad (10).$$

Using the substitutions of $K_0 = k_0 \nu_0$, $E_A = E_{A1} + E_{A2}$, we obtain

$$\frac{dy}{dT} = -K_0 \exp \left[-\frac{E_A}{RT} \right] y \frac{T}{\beta^2} \quad (11).$$

The maximum desorption fraction rate is found by making $d^2y/dT^2=0$, and thus we obtain the relationship

$$\exp \left[-\frac{E_A}{RT} \right] = \frac{\beta^2}{K_0 T^2} \left[\frac{E_A}{RT} + 1 \right] \quad (12).$$

If we assume that $\frac{E_A}{RT} \geq 1$ (usually $E_A / RT \cong 100$), it is possible to put $\frac{E_A}{RT} + 1 \cong \frac{E_A}{RT}$, and then we obtain the following equation,

$$\ln[\beta^2 / T_p^3] = -E_A / RT_p + \ln[K_0 R / E_A] \quad (13).$$

From Eq.(1) for the first order reaction, we similarly obtain the usual Kissinger equation as follows,

$$\ln[\beta / T_p^2] = -E_{A1} / RT_p + \ln[k_0 R / E_{A1}] \quad (14).$$

Using the different Kissinger equations (13) or (14), the activation energy E_A and E_{A1} was estimated for the pure and catalyzed MgH_2 respectively as follows. We measured the TDMS profiles at several heating rates from 1 °C/min to 20 °C /min as a function of temperature for non-catalyzed and Ni^{nano} -catalyzed MgH_2 . The results are plotted in Figs. 10 (a) and (b). From the peak temperature T_p observed at the heating rate of β , the Kissinger plots, i.e., $\ln [\beta^2 / T_p^3]$ and $\ln [\beta / T_p^2]$ as a function of the inverse of T_p are given in Figs. 11 (a) and (b) for non-catalyzed and catalyzed MgH_2 , respectively. From the slope of these straight lines, the activation energies of E_A and E_{A1} were estimated to be 323 ± 40 kJ/mol H_2 and 94 ± 3 kJ/mol H_2 , respectively. The difference value of ~ 230 kJ/mol H_2 between these activation energies indicates the activation energy of E_{A2} corresponding to surface activation process in pure MgH_2 . Thus, Ni^{nano} -catalyzed MgH_2 possessing the activated surface significantly decreases the activation energy of hydrogen desorption.

Fernández et al. [25] also have determined the activation energy in the HD process for the pure MgH_2 by deducing the reaction rate constant k at several different temperatures assuming the Johnson-Mehl-Avrami (JMA) equation for a nucleation and growth process model. The estimated value was ~ 160 kJ/mol H_2 , which is much smaller than our estimated one. This disagreement may be due to the difference between the used models. Because if we adapt the first order reaction model without considering surface activation process, the activation energy is deduced to be 159 ± 20 kJ/mol H_2 using the usual Kissinger plot from our experimental data, which is corresponding to almost the same value with Fernández's estimation.

4. Conclusion

In this work, the hydrogen desorption (HD) properties of the catalyzed MgH₂ composite prepared by mechanically milling the mixture of MgH₂ and a small amount of Fe^{nano}, Co^{nano}, Ni^{nano} and Cu^{nano} nanoparticle metals as a catalyst were carefully examined. All the catalyzed MgH₂ composite showed much better HD properties than the pure milled MgH₂ by only 2h milling. Especially, the 2 mol% Ni^{nano}-doped MgH₂ composite prepared by soft milling for a short milling time of 15 min under a slow milling revolution speed of 200 rpm shows the most superior hydrogen storage properties: The product has a quite sharp peak at ~200 °C in the TDMS curve and a large amount of hydrogen (~6.5 wt.%) is desorbed in the temperature range from 150 to 250 °C under a heating rate of 5 °C /min. The EDX micrographs corresponding to Mg and Ni element profiles indicated that a small amount of nanoparticle Ni^{nano} metals homogeneously dispersed on the surface of MgH₂.

We confirmed that the Ni^{nano}-catalyzed product revealed better reversible hydriding and dehydriding cycles at 150 °C than those at 200 °C, though the 2nd cycle data is slightly worse than that after 1st cycle after milling. This degradation at 200 °C is due to the fact that Mg₂Ni phase grows up in the boundary between MgH₂ phase and Ni catalyst after hydrogen was desorbed at 200 °C. From the studies of kinetics, the HD reactions in non-catalyzed and Ni^{nano}-catalyzed MgH₂ could be understood by the modified first order model, in which the surface activation condition was taken into account.

In addition, from the Kissinger plots, the activation energy was estimated to be 323±40 kJ/molH₂ and 94±3 kJ/molH₂ for the non-catalyzed and the catalyzed MgH₂, respectively. The activation energy of surface activation process on the MgH₂ surface in the HD reaction was estimated to be ~230 kJ/mol, which is the difference value between these activation energies. This indicates that the catalytic effect due to Ni^{nano}-doping significantly decreases the activation energy for hydrogen desorption by surface activation.

ACKNOWLEDGMENT This work was supported by the project “Development for Safe Utilization and Infrastructure of Hydrogen Industrial Technology” in the New Energy and Industrial Technology

Development Organization (NEDO), Japan, and by a Grant-in-Aid for COE Research (No. 13CE2002) of the Ministry of Education, Sciences and Culture of Japan,.

Figure 1. Thermal desorption mass spectra (TDMS) of hydrogen for pure MgH₂ milled for 2 h and catalyzed MgH₂ with 1 mol% Cu^{nano}, Fe^{nano}, Co^{nano} and Ni^{nano} nano-particle metals milled for 2 h at 400 rpm under He gas flow with no partial pressure of hydrogen. In this figure, TDMS profile for MgH₂ with 1 mol% Ni^{micro} micro-particle metals milled for 2 h at 400 rpm are also shown for comparison with that of the 1 mol% Ni^{nano}-catalyzed MgH₂ composite

Figure 2. X-ray diffraction profiles for pure MgH₂ and catalyzed MgH₂ with 1mol% Cu^{nano}, Fe^{nano}, Co^{nano} and Ni^{nano} nano-particle metals milled for 2 h at 400 rpm.

Figure 3. Thermal desorption mass spectra of hydrogen from the MgH₂ composites with 1mol% Ni^{nano} in the milling conditions for 15 min, 1 h, and 2 h at 400 rpm.

Figure 4. Thermal desorption mass spectra of hydrogen for the MgH₂ composites milled for 15 min at (a) 400 rpm with 1mol% Ni^{nano}, (b) 200 rpm with 1mol% Ni^{nano}, and (c) 200 rpm with 2mol% Ni^{nano}, respectively.

Figure 5. EDX micrographs of (a) Mg and (b) Ni elements in the MgH₂ composite with 2 mol% Ni^{nano} prepared by milling for 15 min at 200 rpm.

Figure 6. Thermal desorption mass spectra of hydrogen and TG profiles for the 2 mol% Ni^{nano} catalyzed MgH₂ composite prepared by milling for 15 min at 200 rpm. The solid line is the product after milling for 15 min at 200 rpm, the dashed line is for the sample after the 2nd hydriding/dehydriding cycle at 150 °C and the dotted line for the sample after 2nd cycle at 200 °C.

Figure 7. X-ray diffraction profiles for the 2mol% Ni^{nano}-catalyzed MgH₂ composite prepared (a) after milling for 15 min at 200 rpm, (b) the product after dehydrogenation at 150 °C and (c) the sample after dehydrogenation at 200 °C, respectively.

Figure 8. Weight loss due to hydrogen desorption and the aspect of temperature fluctuation around fixed temperatures as a function of HD reaction time for (a) the 2 mol% Ni^{nano}-catalyzed MgH₂ composite prepared by milling for 15 min at 200 rpm and (b) the pure MgH₂ milled for 15 min at 200 rpm, respectively.

Figure 9. Normalized residual hydrogen function $F(t)$, and the aspect of temperature fluctuation around fixed temperatures as a function of HD reaction time for (a) the 2 mol% Ni^{nano}-catalyzed MgH₂ composite prepared by milling for 15 min at 200 rpm and (b) the pure MgH₂ milled for 15 min at 200 rpm, respectively.

Figure 10. Thermal desorption mass spectra of hydrogen under various heating rates ($\beta=1,5,10,20^{\circ}\text{C}/\text{min}$) from (a) the pure MgH₂ milled for 15 min at 200 rpm and (b) the 2mol% Ni^{nano}-catalyzed MgH₂ composite prepared by milling for 15 min at 200 rpm, respectively. The intensities of longitudinal axis indicates the amount of hydrogen desorption per unit time.

Figure 11. Two kinds of Kissinger plots for the hydrogen desorption reaction for (a) pure MgH₂ milled for 15 min at 200 rpm and (b) the 2mol% Ni^{nano}-catalyzed MgH₂ composite prepared by milling for 15 min at 200 rpm, respectively. Notations: T_p indicates the peak temperatures in thermal desorption spectra (a) and (b) respectively.

REFERENCES and NOTES

- (1) D. L. Cummings, G. J. Powers, Ind. Eng. Chem., Process Des. Develop. **1974**, 13, 182
- (2) J. F. Stampfer, Jr, C.E. Holley, Jr, J. F. Suttle, J. Am. Chem. Soc. **1960**, 82, 3504
- (3) B. Vigeholm, J. Kjoller, B. Larsen, J. Less-Common Met. **1980**, 74, 341
- (4) G. Liang, J. Huot, S. Boily, A. Van Neste and R. Schulz, J. Alloys Comp. **1999**, 291, 295
- (5) G. Liang, J. Huot, S. Boily, A. Van Neste and R. Schulz, J. Alloys Comp. **1999**, 292, 247

- (6) G. Liang, J. Huot, S. Boily and R. Schulz, *J. Alloys Comp.* **2000**, 305, 239
- (7) Z. Dehouche, R. Djaozandry, J. Huot, S. Boily, J. Goyette, T. K. Bose and R. Schulz, *J. Alloys Comp.* **2000**, 305, 264
- (8) J. Huot, J. F. Pelletier, G. Liang, M. Sutton and R. Schulz, *J. Alloys Comp.* **2002**, 330-332, 727
- (9) A. Zaluska, L. Zaluski and J. O. Ström-Olsen, *J. Alloys Comp.* **1999**, 288, 217
- (10) I. Kanoya, M. Hosoe and T. Suzuki, *Honda R & D Technical Review* **2002**, 14, 91
- (11) W. Oelerich, T. Klassen and R. Bormann, *J. Alloys Comp.* **2001**, 315, 237
- (12) W. Oelerich, T. Klassen and R. Bormann, *Adv. Eng. Mater.* **2001**, 3, 487
- (13) Z. Dehouche, T. Klassen, W. Oelerich, J. Goyette, T. K. Bose and R. Schulz, *J. Alloys Comp.* **2002**, 347, 319
- (14) Gagik Barkhordarian, Thomas Klassen and Rüdiger Bormann, *Scripta Materialia* **2003**, 49, 213
- (15) K. Higuchi, K. Yamamoto, H. Kajioka, K. Toiyama, M. Honda, S. Orimo, H. Fujii, *J. Alloys Comp.* **2002**, 330-332, 526
- (16) H. Fujii, K. Higuchi, K. Yamamoto, H. Kajioka, S. Orimo, K. Toiyama, *Materials Trans.* **2002**, 43, 2721
- (17) O. Gutfleisch, N. Schlorke-de Boer, N. Ismail, M. Herrich, A. Walton, J. Speight, I. R. Harris, A. S. Pratt and A. Züttel, *J. Alloys Comp.* **2003**, 356-357, 598
- (18) J-L. Bobet, B. Chevalier, M.Y. Song, B. Darriet, J Etourneau, *J. Alloys Comp.* **2003**, 336, 292
- (19) Nobuko hanada, Takayuki Ichikawa, Shin-Ichi Orimo, Hironobu Fujii, *J. Alloys Comp.* **2004**, 366, 269
- (20) J. Harris, S. Andersson, *Phys. Rev. Lett.*, **1985**, 55, 1583

- (21) M. Avrami. J. Chem. Phys. **1939**, 7, 1103.
- (22) M. Avrami. J. Chem. Phys. **1940**, 8, 212.
- (23) M. Avrami. J. Chem. Phys. **1941**, 9, 177
- (24) J. Huot, G. Liang, S. Boily, A. Van Neste, R. Schulz, J. Alloys Comp. **1999**, 293-295, 495
- (25) J.F. Fernández, C.R. Sánchez, J. Alloys Comp. **2002**, 340, 189
- (26) L. Schlapbach(Ed.), Hydrogen in Intermetallic Compounds 2, Springer-Verlag, 1992, p. 178
- (27) H.E. Kissinger, Anal. Chem. **1957**, 29, 1702.

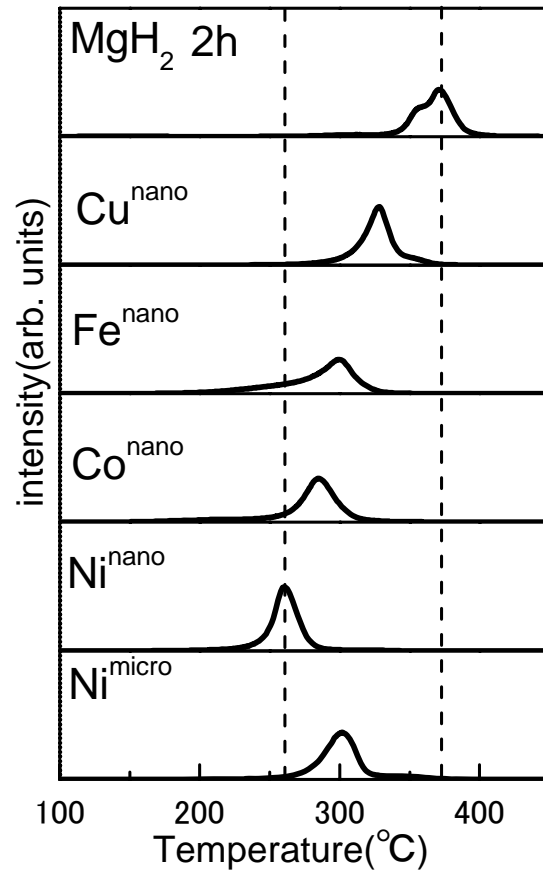


Figure 1.

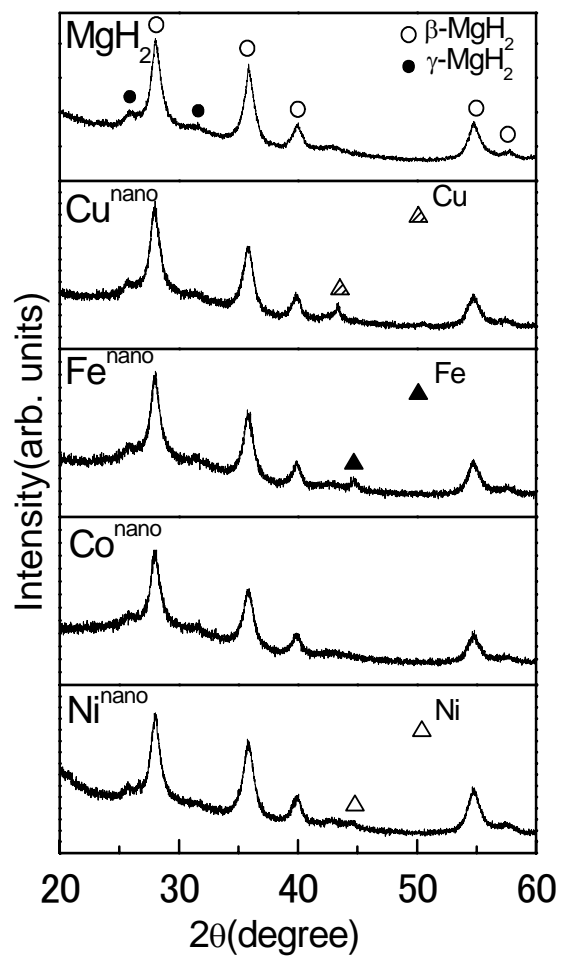


Figure 2.

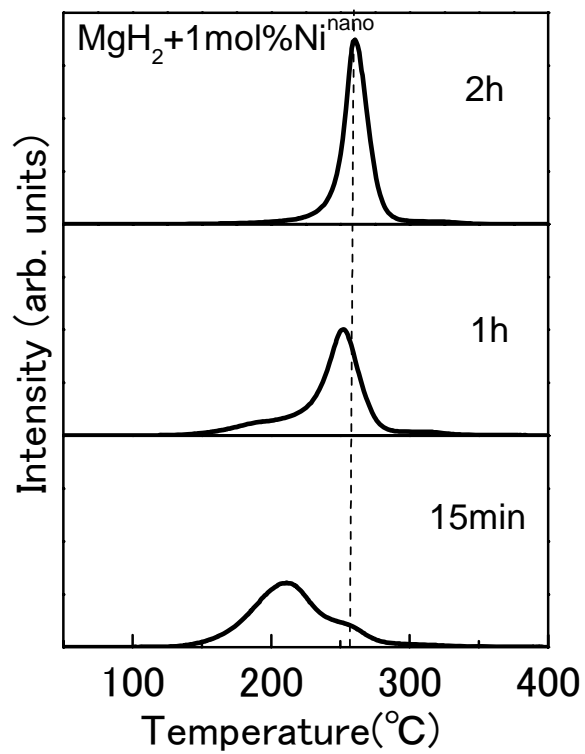


Figure 3.

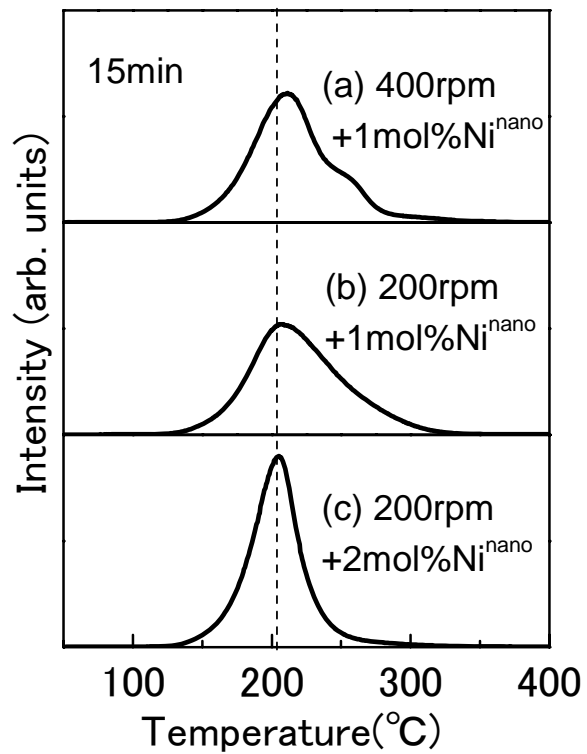


Figure 4.

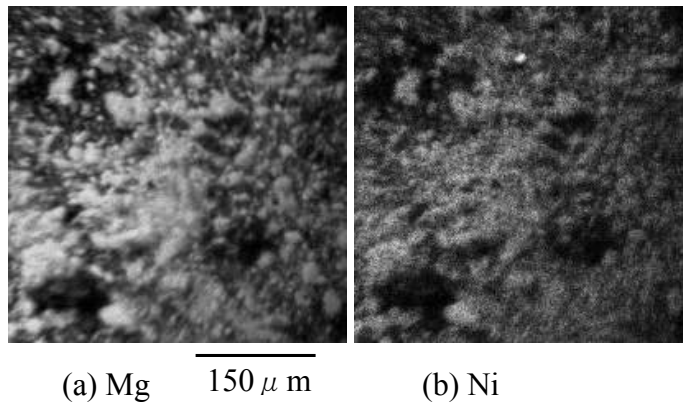


Figure 5.

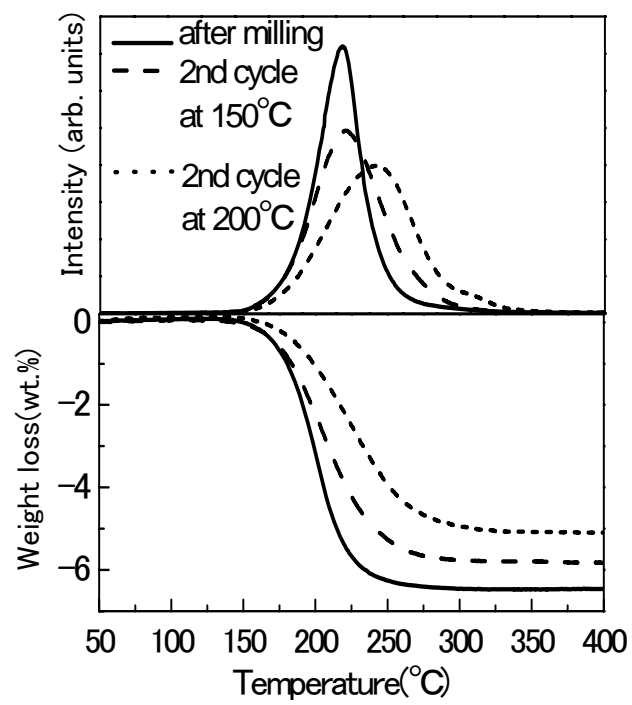


Figure 6.

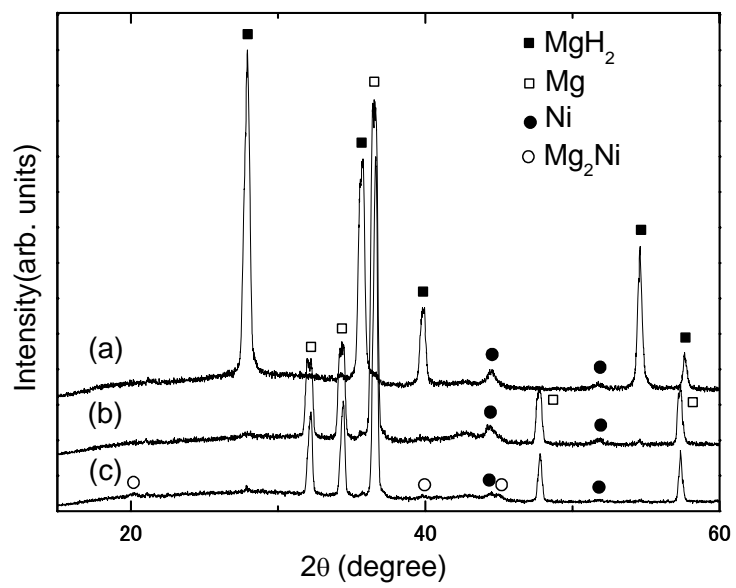
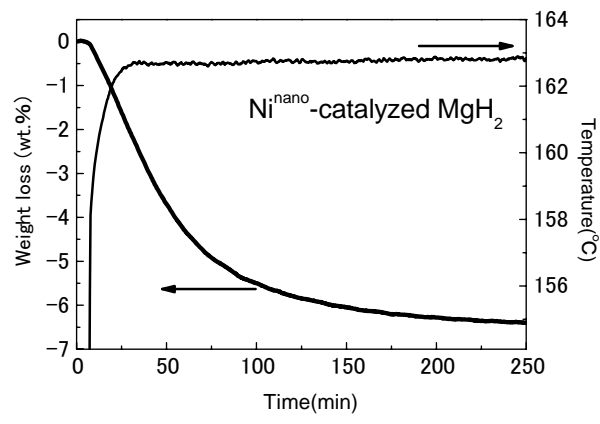
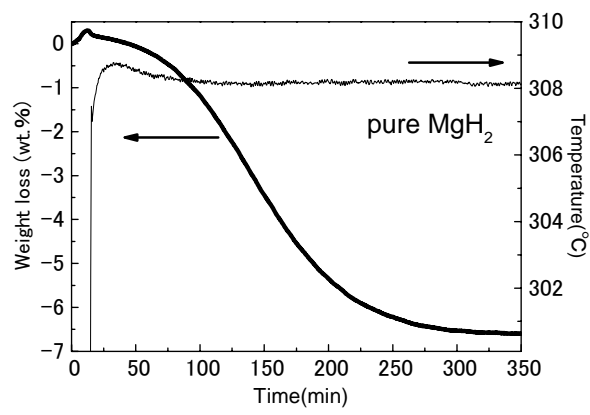


Figure 7.

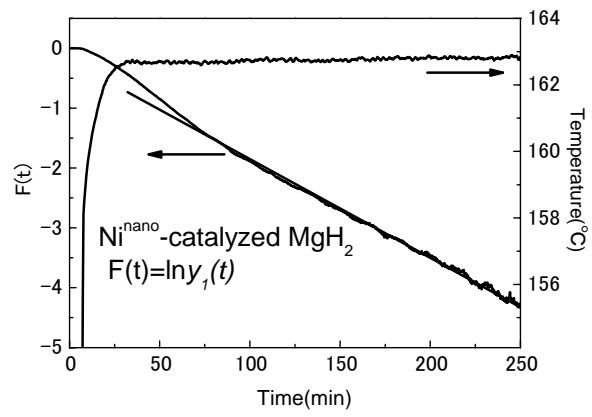


(a)

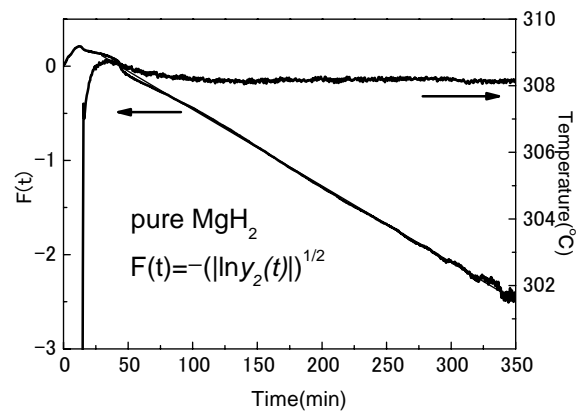


(b)

Figure.8

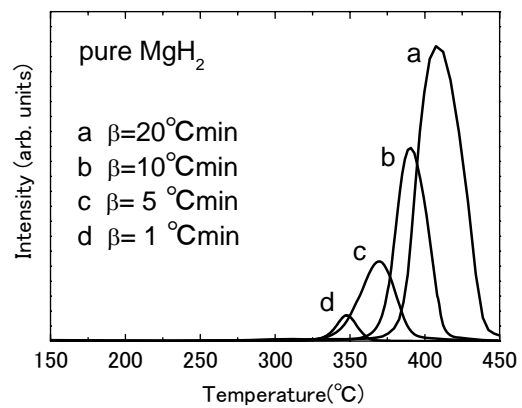


(a)

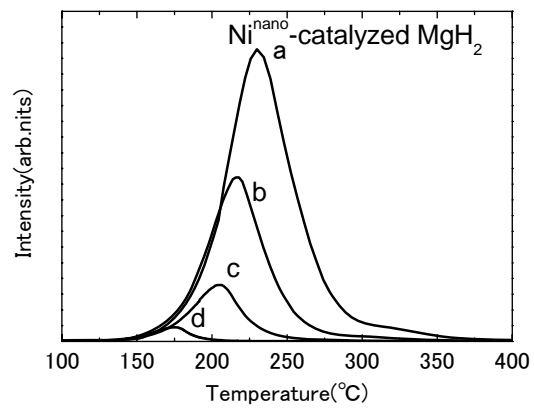


(b)

Figure.9

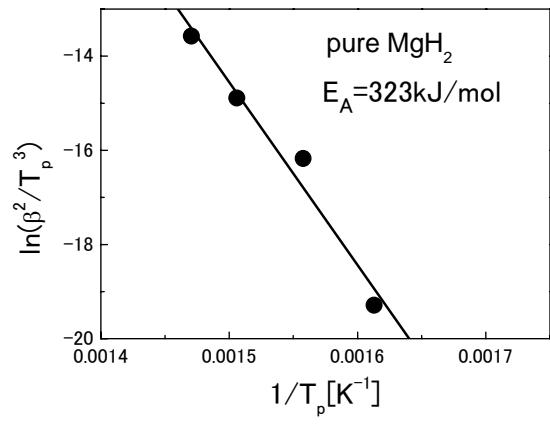


(a)

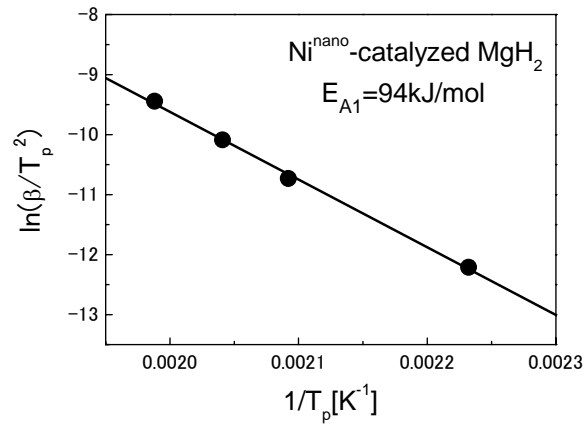


(b)

Figure 10.



(a)



(b)

Figure 11.